Atmos. Meas. Tech. Discuss., 8, 7879–7907, 2015
www.atmos-meas-tech-discuss.net/8/7879/2015/
doi:10.5194/amtd-8-7879-2015

Atmospheric Measurement Techniques Discussions
Open Access

Coded continuous wave meteor radar

J. Vierinen[1], J. L. Chau[2], N. Pfeffer[2], M. Clahsen[2], and G. Stober[2]

[1]MIT Haystack Observatory, Route 40 Westford, 01469 MA, USA
[2]Leibniz Institute of Atmospheric Physics (IAP), Schloss Str. 6, 18225 Kühlungsborn, Germany

Received: 29 June 2015 – Accepted: 8 July 2015 – Published: 30 July 2015

Correspondence to: J. Vierinen (x@mit.edu)

Published by Copernicus Publications on behalf of the European Geosciences Union.

Abstract

The concept of coded continuous wave meteor radar is introduced. The radar uses a continuously transmitted pseudo-random waveform, which has several advantages: coding avoids range aliased echoes, which are often seen with commonly used pulsed specular meteor radars (SMRs); continuous transmissions maximize pulse compression gain, allowing operation with significantly lower peak transmit power; the temporal resolution can be changed after performing a measurement, as it does not depend on pulse spacing; and the low signal to noise ratio allows multiple geographically separated transmitters to be used in the same frequency band without significantly interfering with each other. The latter allows the same receiver antennas to be used to receive multiple transmitters. The principles of the signal processing are discussed, in addition to discussion of several practical ways to increase computation speed, and how to optimally detect meteor echoes. Measurements from a campaign performed with a coded continuous wave SMR are shown and compared with two standard pulsed SMR measurements. The type of meteor radar described in this paper would be suited for use in a large scale multi-static network of meteor radar transmitters and receivers. This would, for example, provide higher spatio-temporal resolution for mesospheric wind field measurements.

1 Introduction

Scattering of radio waves from plasma structures created by meteoroids burning in the Earth's atmosphere were early on recognized important for not only radio propagation, but also remote sensing of meteoroids and the atmosphere with which the meteoroids interact with (McKinley, 1961b; Sugar, 1964).

The main categories of meteor radio scattering phenomena are known to be: specular scattering from the enhanced electron density left suspended in the atmosphere behind the ablating meteroid (Sugar, 1964); non-specular trails echoes, which are caused

AMTD
8, 7879–7907, 2015

by Bragg scattering from ionospheric irregularities that form in the wake of the ablating meteoroid (Dyrud et al., 2002; Chau et al., 2014); and finally meteor head echoes, which are echoes from the area around the ablating meteor which has an electron density higher than the plasma frequency of the scattering radio wave (Evans, 1966; Pellinen-Wannberg and Wannberg, 1994).

Of these types of scattering, the specular and non-specular trails have large enough radar cross-sections at VHF frequencies that they can be regularly observed with a small < 1 kW average transmit power meteor radar with a collecting area consisting of typically five nearly isotropically radiating receiver antennas and one nearly isotropically radiating transmit antenna. Specular and non-specular trail echoes are used to sense the mesospheric neutral wind (Holdsworth et al., 2004), temperature (Hocking, 1999), as well as trajectories of the meteoroids entering the Earth's atmosphere (Jones et al., 2005).

Commonly used meteor radars typically use short pulsed transmission with peak power of approximately 15 kW and a pulse repetition rate of 300–2144 pulses per second (Hocking et al., 2001b). The meteor trails are typically point-like in range, have Doppler shift of < 20 Hz, and correlation times ranging from few hundred milliseconds to few tens of seconds. Due to the long correlation time, these targets are highly suitable for amplitude domain coherent processing, which results in an increase in signal to noise ratio linearly dependent on the time that the signal can be integrated (Markkanen et al., 2005), assuming that we can match the Doppler and angle of arrival characteristics in some way. This coherent integration can be maximized if continuous transmissions are used. For example, a continuous transmission would result in ≈ 14 dB of increased signal processing gain when compared to a pulsed system with a duty-cycle of 4.4 %. This additional gain can be either used to increase the fidelity of measured signals, or to reduce the peak transmit power requirements of a meteor radar system, in order to e.g., reduce the cost of a radar system.

Long coded transmissions are a well established method for radar transmission coding. They can be used for planetary radar (Evans and Hagfors, 1968), for stratospheric

AMTD
8, 7879–7907, 2015

radar (Woodman, 1980), and also for incoherent scatter radar (Sulzer, 1986; Lehtinen and Häggström, 1987). In these cases, the radar transmissions are either coded with a pseudo-random binary phase code, or some optimized phase code (Vierinen et al., 2008) that can be used to unambiguously decode the radar echoes by using the property that the range sidelobes of the radar target are either analytically zero or statistically approach zero.

Another example of a system that uses coded continuous wave radio transmissions is the Global Positioning System (GPS) (Hofmann-Wellenhof et al., 2013). It utilizes coded sequences, which are unique for each satellite. This allows each satellite to use the same frequency, which simplifies many aspects of calibration and receiver design. The concept of sharing the spectrum between multiple independent users is a well known design paradigm in telecommunications engineering known as Code Division Multiple Access (CDMA). This same concept can also be used for meteor radar to enable a multi-static meteor radar system that operates with the same frequency.

Multi-static meteor radars have been shown to be useful not only for astronomical measurements of meteor radiants (Jones et al., 2005; Fritts et al., 2010), but also for higher spatiotemporal resolution in measurements mesospheric winds (Stober and Chau, 2015). A multi-static network of transmitters and receivers allows more specular meteor trails to be measured in the same geographic area. The reason is that there are more possibilities for the specular condition to be matched for a meteor trail when there are more transmitter-receiver combinations.

Bi-static scattering also has the advantage that it effectively uses longer Bragg wavelengths than a mono-static radar that uses the same radar transmit frequency. In this case of forward scatter, the Bragg vector is obtained from the difference of the incident and scatter wave vectors, which results in effectively a longer Bragg wavelength. This has the effect of lifting the meteor ceiling (McKinley, 1961a), allowing observing more echoes at higher altitudes where the ionization efficiency is lower than with a mono-static radar operating on the same wavelength.

AMTD
8, 7879–7907, 2015

One inhibitive factor in the use of multi-static systems has been cost. The feasibility of multi-static SMRs to improve MLT wind measurements has been tested by Stober and Chau (2015) with the MMARIA (Multistatic and Multifrequency Agile Radar for Investigations of the Atmosphere) concept. They proposed adding the capability to receiver multiple transmitters with the same receiver. The cost could be further reduced, if the same receive antennas could be used to observe multiple transmitters operating at the same frequency simultaneously. Using the same frequency would also simplify interferometry with spaced antennas. Additionally, if a lower peak power were used on transmitters, the cost of a transmitter would also be further reduced. This is the motivation for using the idea of coded continuous wave (CW) transmissions for SMRs, which we describe in this paper.

We will first discuss an overview of the concept of a CDMA network of meteor radar transmitters and receivers. We will then go through mathematical signal processing methods for radar target estimation using coded continuous wave measurements, going through several special cases and practical considerations. Then we show measurements obtained during a recent campaign to demonstrate the applicability of the method. Finally, we discuss our results, outline the resulting capabilities, future plans, and suggest several other potential radio remote sensing applications to the coded continuous wave method.

2 Multi-static meteor radar network

The number of detected specular meteor trails using a multi-static meteor radar network can be estimated with $N \approx c(d)N_0N_{TX}N_{RX}$, where N_0 is the number of meteors detected with a monostatic system, N_{TX} is the number of transmitter stations, N_{RX} is the number of receiver stations and $c(d)$ is a factor that depends on range between transmitter and receiver. The longer the distance, the smaller this value gets. Typically this factor is between between 0.3 and 0.8. This estimate can be used as a guideline when e.g., determining the cost per detection of a meteor trail within a multi-static

AMTD
8, 7879–7907, 2015

meteor radar network. There are also other factors that determine the performance of a multi-static meteor radar system, but these will not be discussed in this study.

For example, consider the following network: five receiver antenna fields with five receiver antennas each, and ten transmitters, each with a single antenna. In this network, there are 35 antennas in total, but it observes approximately the number of meteors that 25 independent mono-static systems would, assuming $c(d) = 0.5$. However, 25 mono-static meteor radar systems would require 150 antennas in total. Assuming that the cost of the system is proportional to the number of antennas, the multi-static system would be more efficient by a factor of 4.3 than a network of mono-static radars.

3 Signal processing

The key to coded continuous wave radar measurements is deconvolution of echoes from coded transmissions. This can be performed either in frequency domain where discrete Fourier transforms can be used to speed up computations, or in time domain, where more computationally expensive full matrix representation of the measurement equations is needed. In order to achieve more flexibility in selection of temporal resolution and the range gates that are to be analyzed, we will describe the time domain approach, which leads to a linear measurement equation and linear-least squares estimation procedure. The linear measurement equations are also more general, as they can be used to model e.g., multiple transmitters, or to deal with missing measurements.

3.1 Coherent deconvolution with linear least-squares

Meteor trail echoes are associated with very small Doppler shifts due to the neutral wind. Given a short enough time period, the complex target scatter coefficient can be assumed to be constant. Even though a single meteor is a point target, multiple meteor echoes are often observed simultaneously. There are also many cases where meteor echoes can spread in range. Therefore, it is beneficial to treat our unknown as a range

AMTD
8, 7879–7907, 2015

spread coherent radar target. The coherence assumption is made by assuming that the target scatter as constant over L samples. We will refer to this as the coherence time. Given these considerations, our measurement equation is as follows:

$$m_t = \sum_{r=0}^{R} \epsilon_{t-r} \zeta_{r,i} + \xi_t, \tag{1}$$

where $\epsilon_t \in \mathbb{C}$ is the radar transmission waveform, $\zeta_{r,i} \in \mathbb{C}$ is the target backscatter coefficient at a given range gate and coherence time i. Receiver noise is modeled with $\xi_t \in \mathbb{C}$. We assume that it is a proper complex Gaussian random process $\xi_t \sim N_{\mathbb{C}}(0, \Sigma)$.

In a multi-static measurement with multiple transmitters operating on the same center frequency, there can be multiple different propagation paths that are simultaneously actively probed by a certain receiver. In order to differentiate between transmitters, each transmitter should have a different transmit waveform $\epsilon_{t,k} \in \mathbb{C}$. We use $k \in [0, N] \in \mathbb{N}$ to index the transmitters. In this case the measurement equation is a sum of convolutions, with one convolution for each transmitter-receiver pair received by a single station

$$m_t = \sum_{k=0}^{N} \sum_{r=0}^{R} \epsilon_{t-r,k} \zeta_{r,i,k} + \xi_t, \tag{2}$$

where also the scatter is different for each transmitter-receiver propagation path $\zeta_{r,i,k} \in \mathbb{C}$.

Let us first write the inner sum of this equation in matrix form:

$$\boldsymbol{m}_i = \sum_{k=0}^{N} \mathbf{A}_{i,k} \boldsymbol{x}_{i,k} + \boldsymbol{\xi}_i, \tag{3}$$

where the unknown parameters, i.e., radar echoes from transmitter k and time $t \in [iL, (i+1)L - 1]$ are $\boldsymbol{x}_{i,k} = [\zeta_{0,i,k}, \cdots, \zeta_{R,i,k}]^{\mathrm{T}} \in \mathbb{C}^R$, and the measurement vector is $\boldsymbol{m}_i =$

AMTD
8, 7879–7907, 2015

$[m_{iL}, m_{iL+1}, \cdots, m_{(i+1)L-1}]^{\mathrm{T}} \in \mathbb{C}^{L}$. Here the theory matrix $\mathbf{A}_{i,k} \in \mathbb{C}^{L \times R}$ providing the linear relation between echoes for a single transmitter k and the measurements is Toeplitz formed:

$$\mathbf{A}_{i,k} = \begin{bmatrix} \epsilon_{iL,k} & \epsilon_{iL-1,k} & \cdots & \epsilon_{iL-R,k} \\ \epsilon_{iL+1,k} & \epsilon_{iL+1-1,k} & \cdots & \epsilon_{iL+1-R,k} \\ \vdots & \vdots & \ddots & \vdots \\ \epsilon_{(i+1)L-1,k} & \epsilon_{(i+1)L-1-1,k} & \cdots & \epsilon_{(i+1)L-1-R,k} \end{bmatrix}. \quad (4)$$

This is depicted in form of a range-time diagram in Fig. 2.

Equation (3) can be expressed as an equation with just a single matrix

$$\boldsymbol{m}_i = \mathbf{A}_i \boldsymbol{x}_i + \boldsymbol{\xi}_i \quad (5)$$

where the theory matrix is a set of stacked convolution matrices:

$$\mathbf{A}_i = [\mathbf{A}_{i,0}, \cdots, \mathbf{A}_{i,N}] \quad (6)$$

and the unknown vector is a set of stacked parameter vectors $\boldsymbol{x} = [\boldsymbol{x}_{i,0}^T, \cdots, \boldsymbol{x}_{i,N}^T]^T$.

The maximum likelihood estimate for the unknown parameters, i.e., echoes for all the range gates and all transmit-receiver pairs can be obtained using the standard formula for complex linear least-squares problems:

$$\boldsymbol{x}_{i,\mathrm{ML}} = (\mathbf{A}_i^{\dagger} \boldsymbol{\Sigma}^{-1} \mathbf{A}_i)^{-1} \mathbf{A}_i^{\dagger} \boldsymbol{\Sigma}^{-1} \boldsymbol{m}_i, \quad (7)$$

which is solvable as long as $\mathbf{A}_i^{\dagger} \boldsymbol{\Sigma}^{-1} \mathbf{A}_i$ is not singular. Here † is the Hermitian operation, i.e., a conjugate and transpose. With several transmitters this is often the case, if transmitters use e.g., pseudorandom sequences and there are more measurements than unknowns $L \geq NR$. Code optimality is determined by how good the a posteriori covariance matrix is: $\boldsymbol{\Sigma}_{\mathrm{post}} = (\mathbf{A}_i^{\dagger} \boldsymbol{\Sigma}^{-1} \mathbf{A}_i)^{-1}$. For a single transmitter-receiver case, Frank and Chu codes (Frank, 1973) are known to be perfect, i.e., they result in the smallest possible constant diagonal value of $\boldsymbol{\Sigma}_{\mathrm{post}}$.

AMTD
8, 7879–7907, 2015

3.2 Treating other transmissions as noise

If each station utilizes a different pseudorandom transmit waveform that is statistically orthogonal from one another, i.e., $E\epsilon_{t,k}\epsilon^*_{t',k'} = 0$ for all t and t' when $k \neq k'$ and $E\epsilon_{t,k}\epsilon^*_{t',k'} = 0$ for all k and k' when $t \neq t'$, one can analyze the multi-static measurements by assuming that there is only one transmitter, and the signals from other transmitters is additive noise

$$\boldsymbol{m}_i = \mathbf{A}_{i,k}\boldsymbol{x}_{i,k} + \boldsymbol{\xi}'_i, \tag{8}$$

where $\boldsymbol{\xi}'_i = \boldsymbol{\xi}_i + \sum_{k' \neq k}\mathbf{A}_{i,k'}\boldsymbol{x}_{i,k'}$. If the radar echoes have a low signal to noise ratio, then we can assume that $\boldsymbol{\xi}'_i \sim N_{\mathbb{C}}(0, \boldsymbol{\Sigma})$ and that $\boldsymbol{\xi}'_i \approx \boldsymbol{\xi}_i$ because the echoes from other transmitters do not significantly contribute to the receiver noise. This allows us to treat each transmit-receive pair an independent radar measurement. This significantly simplifies the estimation problem for large scale multi-static networks. In this case, the maximum likelihood estimate for each transmitter-receiver pair is obtained with theory matrix $\mathbf{A}_{i,k}$ used in Eq. (7).

With high signal to noise ratio, using the signal propagation path model in Eq. (8) is not as accurate. But even then, the effect of not modeling the echoes from other transmissions properly only results in an increase in the the variance of the estimates. If the radar transmit waveform is considered as a zero-mean random variable, then the error term $\boldsymbol{\xi}'$ is also a zero mean random process, and the linear least-squares estimator still provides an unbiased estimator, albeit not the most optimal one.

3.3 Numerically efficient solution

In the previous sections, we did not restrict the waveform in any way, although we mention that pseudorandom waveforms are good waveforms to use. In practice, from a numerical point of view, there are good reasons to design a waveform in such a way that it repeats after a short enough period of time.

AMTD
8, 7879–7907, 2015

If our continuous code repeats exactly at the coherence length L, it is possible to precalculate the computationally intensive portion of the linear-least squares estimator:

$$\mathbf{B} = (\mathbf{A}^{\dagger}\mathbf{\Sigma}^{-1}\mathbf{A})^{-1}\mathbf{A}^{\dagger}\mathbf{\Sigma}^{-1}. \quad (9)$$

The maximum likelihood estimate for target backscatter can then be obtained with $\boldsymbol{x}_{\mathrm{ML}} = \mathbf{B}\boldsymbol{m}$. If the coherence assumption L is shorter than the length of the repeating pseudorandom sequence L_s, the maximum likelihood can still be precalculated, but there have to be L_s/L precalculated matrices $\mathbf{B}_i \in \mathbb{C}^{NR\times L}$ that cycle through, assuming that there are an integer number of coherence lengths in the pseudorandom cycle length $i \in [1, L_s/L]$.

With a precalculated maximum likelihood estimation matrix, the deconvolution can be performed significantly faster than real-time with a modern personal computer. Our deconvolution software is currently implemented with Python script that uses Numeric Python, and cannot be considered highly optimized. This software can easily keep up with five receive channels at receive bandwidths of around 100 kHz and 10 µs range gates up to 1500 km.

3.4 Bursty interference

When using the matrix method for analyzing target echoes, it is possible to deal with bursty interference from nearby power-line interference or a radar using short transmit pulses. The rows corresponding to bad measurements can be detected using a statistical outlier test and simply removed from the theory matrix and measurement vector. This method works as long as $\mathbf{A}^{\dagger}\mathbf{\Sigma}^{-1}\mathbf{A}$ is not singular. This is typically the case if there are more measurements than unknown parameters. Leaving out rows with time localized interference however prevents the use of a precalculated maximum likelihood estimation matrix, which results in a numerically less efficient solution for the target scatter estimate.

AMTD
8, 7879–7907, 2015

3.5 Target detection

When detecting targets, we assume that each target is point-like and has a Doppler shift. Specular echoes have very small range migration, which means that we can assume them to be at a fixed range gate. The following equation can be used for as a model when detecting targets:

$$m_{a,t} = \epsilon_{t-r}\sigma\gamma_a(\alpha,\phi)e^{i\omega t} + \xi_t \tag{10}$$

where $m_{a,t} \in \mathbb{C}$ is the complex baseband voltage received with antenna $a \in \mathbb{N}$, $\sigma \in \mathbb{C}$ the complex scattering coefficient, $\gamma_a(\alpha,\phi) \in \mathbb{C}$ is the direction of arrival dependent delay as complex phase with azimuth $\alpha \in [0, 2\pi] \subset \mathbb{R}$ and elevation $\phi \in [0, \pi/2] \subset \mathbb{R}$; $\omega \in \mathbb{R}$ is Doppler shift $\xi_t \sim N_{\mathbb{C}}(0, b\mathbf{I})$ is measurement noise, which is proper complex Gaussian white noise. In matrix form this is

$$\boldsymbol{m} = \mathbf{A}_\theta \boldsymbol{x} + \boldsymbol{\xi}, \tag{11}$$

where $\boldsymbol{m}$ is a vector of measured complex baseband voltages from all antennas. The moving point target model parameters are $\boldsymbol{\theta} = [\omega, r, \alpha, \phi]^T$. The vector $\boldsymbol{x} = [\sigma]^T$ is a single element vector containing the complex target scatter coefficient.

This is a non-linear inverse problem with a probability density function proportional to

$$p(\boldsymbol{m}|\boldsymbol{\theta}, \boldsymbol{x}) \propto \exp\left\{-\|\mathbf{A}_\theta \boldsymbol{x} - \boldsymbol{m}\|^2\right\}. \tag{12}$$

The peak of this distribution, i.e., the maximum likelihood estimator for target parameters $\boldsymbol{\theta}$ is

$$\boldsymbol{\theta}_{\mathrm{ML}} = \mathrm{argmax}_\theta |\mathbf{A}_\theta^\dagger \boldsymbol{m}|, \tag{13}$$

which has been shown for moving point targets by e.g., Markkanen et al. (2005) for space debris. In practice, this estimate is found using a sufficiently dense grid search in parameter space for range, Doppler, and angle of arrival.

AMTD
8, 7879–7907, 2015

4 Juliusruh–Kühlungsborn experiment

In order to test the principle of coded CW meteor radar in practice, we performed a bi-static measurement campaign between 18:00 UTC 10 June 2015 and 09:00 UTC 12 June 2015.

In this experiment, the transmitter station was located in Juliusruh (54°37′17.548″ N, 13°22′15.675″ E) and the receiver system is located in Kühlungsborn (54°08′48.665″ N, 11°44′31.209″ E). The locations of the transmitter and receiver are shown in Fig. 3. The same bistatic configuration has been used in Stober and Chau (2015)

4.1 Measurement setup

For this experiment we used a 1000 baud long binary phase code with pseudorandom bits. The baud length was 10 µs and the code was sent continuously in a repeated fashion to allow the use of a numerically efficient precalculated maximum likelihood estimation matrix in the analysis. The sent waveform was generated with a PC, with Gaussian pulse shaping performed with a FIR filter.

The signal is then transferred over a 1 Gb Ethernet connection to a USRP-N200 software defined radio, which converts the digital baseband signal to an analog signal centered at 32.55 MHz with a 100 kHz bandwidth. The USRP N200 was synchronized to the global reference clock using a Trimble Thunderbolt GPS disciplined oscillator (GPSDO).

The signal generated by the USRP N200 was then amplified to 30 W of continuous power and fed through a low pass filter to suppress harmonic emissions. The 30 W signal was fed to the three element yagi transmit antenna of the Juliusruh SKiYMET meteor radar. Only one linear polarization component was used.

In Kühlungsborn, the signals were received with five yagi antennas arranged in a so-called Jones configuration (Jones et al., 1998). These are the same antennas that are used routinely as a bi-static receiver for the Juliusruh pulsed SKiYMET meteor radar. The receiving antennas were configured to receive circular polarization. The five

AMTD
8, 7879–7907, 2015

channels were recorded using a five channel USRP N200 receiver setup, which was synchronized to a global reference using a Trimble Thunderbolt GPSDO. The receivers were synchronized to one another using a 1 PPS and 10 MHz signal from the GPSDO. The five channels were recorded at a 1 MHz bandwidth and further FIR filtered and decimated to 100 kHz using a Gaussian pulse shaping filter to reduce out of band emissions. The signals were recorded to an external hard drive for off-line processing.

4.2 Results

In order to ascertain the performance of our low power coded CW meteor radar concept, we compare the results from our bi-static campaign with existing SKiYMET operational pulsed SMR measurements. First we compare the distributions of some selected parameters obtained during 24 h of operations between our CW and a standard pulsed experiment, operating on the same bi-static configuration. Since the same antennas were used, a simultaneous comparison is not possible. However, as we show below, the comparisons are meaningful. Second, we compare the winds obtained with the coded CW measurements with those obtained from the monostatic SMR system located in Collm (Jacobi, 2006), ∼ 350 km South from our Juliusruh–Kühlungsborn observations.

In Fig. 4, we show selected results of the CW experiment conducted on 11 June 2015: (a) meteor count as a function of time of the day, (b) signal-to-noise (SNR) distributions, (c) Doppler velocity distribution, (d) bivariate distribution of angle of arrival of echoes, as function of direction cosines in x (West to East) and y (South to North) directions; and (e) altitude distributions. These parameters have been obtained on the detected echoes, which were detected with the improved detection schemes described in Sect. 3.5. After detection, the parameter estimation has been done following with the procedures described in Hocking et al. (2001a) and Holdsworth et al. (2004). We show the results of all the possible meteor-like echoes detected above 140 km total range (i.e., 70 km for a roundtrip monostatic range), since range-aliased meteor echoes are not expected in this coded CW experiment.

AMTD
8, 7879–7907, 2015

The results obtained few days earlier (4 June 2015) with a pulsed SMR, using the same bistatic configuration, are shown in Figs. 5 and 6. These measurements have been obtained with a 15 kW peak power transmitter, 625 Hz pulse repetition frequency (i.e., maximum total unambigous range of 480 km) and 10 µs sampling. The results are obtained using the same identification procedure used with the CW data, while the detection is the standard detection used in our operational pulsed-Doppler systems. In Fig. 5, we show the results of all meteor-like echoes before cleaning. The results after a cleaning procedure including the selection of echoes with underdense characteristics are shown in Fig. 6. The cleaning procedure consist mainly on removing those echoes that do not present clear underdense characteristics (Holdsworth et al., 2004), or are outside the expected altitude range between 70 and 120 km. Most of the echoes that have been removed, are caused either by pulsed interferences, non-specular meteor echoes, and airplane echoes. Note that specular meteors echoes coming from ranges above 480 km, will be range aliased into lower ranges, where ground and airplane echoes occur.

By comparing Figs. 5 and 6, we can clearly see that many non-meteor echoes were originally detected. They are clearly visible as narrow distributions in all the plots, but more pronounced in the bivariate direction cosine distributions (i.e., coming from specific locations) and in the velocity distributions (showing larger Doppler shifts than expected).

The results of the CW experiment are in very good quantitative agreement with the results of the pulsed configuration after cleaning. Both show a similar diurnal pattern, with a maximum count of ~ 200 meteors in half-hour bins, the Doppler velocity distributions are also comparable, as well as the bivariate direction cosine and altitude distributions. In the case of the SNR, qualitatively the comparison is good and as expected, i.e., with increasing count as the SNR decreases. Since SNR is a relative quantity (depending on how the noise is treated), we do not focus on the actual number. Instead we observe that with the detection procedures used, specular meteor echoes are detected when SNRs are greater than ~ 0 and ~ -6 dB in the CW and pulsed systems, respec-

AMTD
8, 7879–7907, 2015

tively. A more fair comparison would have been to use the same detection procedures in both datasets (e.g., using the Doppler grid search used in the CW experiment also in the pulse system). However, we have preferred to compare existing procedures in a standard pulsed-system, against the improvements in both transmission as well as in signal processing in the proposed CW system.

To further show the good quality of our CW results, in Fig. 7 we present the derived winds obtained with the CW experiment: zonal and meridional (bottom) wind. The winds are derived using the approach outlined in Hocking et al. (2001a); Holdsworth et al. (2004); Stober et al. (2012), i.e., assuming a horizontal homogeneity of the horizontal wind in the observed volume. The resulting winds show typical summer conditions for a northern mid-altitude station with the expected wind reversal at around 90 km altitude in the zonal flow. Further, both wind components show a strong semi diurnal oscillation.

The winds observed during the same time with the Collm system are shown in Fig. 8. As there is no direct overlap between both observation volumes, it is not expected to get a one by one correspondence of the measured zonal and meridional winds. However, the main general features observed with the CW system are also observed with the Collm system.

5 Discussion

The main advantages of a coded CW SMR are: (a) it can operate with less peak power, (b) it is suitable for a large scale multi-static radar network, (c) it does not suffer from the range-Doppler ambiguity problem, (d) there is no inherent limit to time resolution, and (e) it is less susceptible to false detections due to radio interference when compared with pulsed systems. The latter is possible since the pulse-like interferences would be spread in range and Doppler in the decoding process. We would like to stress the suitability for a large scale-multi-static radar network. Not only would the low power transmitting systems with coded wave forms be more friendly with other radio users

AMTD
8, 7879–7907, 2015

in nearby-bands, but also the receiving systems could be simplified, by allowing the reception of multiple transmitters on the same antenna and same frequency. The separation of the different transmitted signals would be done by knowing the code of each transmitter site.

We have shown that with modest CW system transmitting 30 W average power, one can obtain results not too different from those obtained with standard pulsed transmitter. Already the existing prototype used to demonstrate the principle of coded CW SMR could be used to derive winds in the mesosphere and lower thermosphere. We expect that better results, i.e., more meteor counts, could be easily obtained by increasing the transmitter power; or by adding more transmitters and receivers to measure the same volume.

The same coded CW radar could be used to observe other types of coherent echoes. Although the analysis of such echoes is not fully explored in this paper, we will discuss how these echoes could be measured and analyzed a coded CW system.

While meteor radars observe meteor head echoes much more seldomly than meteor trails, they can still be observed often enough to yield meaningful science on the orbital parameters of meteoroids (Janches et al., 2014). Meteor head echoes have large Doppler shifts. In this case, the deconvolution of coherent echoes does not work, as the assumption of constant phase and amplitude of backscatter during a pulse compression period is not valid. However, these cases could be analyzed with two other approaches: a filter matched in Doppler and range (Markkanen et al., 2005), or using a using sparse model of the target in range-Doppler space (Volz and Close, 2012). Coded CW radar transmit waveforms are highly suited for both of these cases.

Small coherent scatter radars (including SMRs) can also observe echoes from non-specular meteor echoes, E region field-aligned irregularities (Hysell et al., 2004; Hysell and Chau, 2001), or other interesting phenomena such as the meteor radar observations of the failed Russian missile experiment (Kozlovsky et al., 2014). Non-specular meteor echoes could also be due to field-aligned irregularities or charged dust (Chau et al., 2014). Some of these echoes can have a large range and Doppler spread, which

AMTD
8, 7879–7907, 2015

often makes their analysis problematic with pulsed radars with high pulse repetition rate measurements, which are designed for a point target at altitudes between 70 and 120 km. A coded CW transmit waveform would be more suitable for these types of measurements of opportunity, without the range-Doppler ambiguity. With coded CW, even highly overspread targets can be analyzed using lag-profile inversion (Virtanen et al., 2008), provided that a suitable coded continuous waveform is used. Pseudorandom phase coded waveforms are known to be suitable for lag-profile inversion (Sulzer, 1986; Vierinen et al., 2008), allowing the full range of Doppler frequencies measured by the receiver (in the case of 100 kHz receiver bandwidth ±50 kHz) to be analyzed if necessary.

One downside for coded continuous wave meteor radar is that the transmitter cannot be co-located with the receiver antenna. Some separation between transmitter and receivers is needed to avoid saturation of the receivers. We do not know the minimum distance needed to avoid saturation for typical meteor radar receiving antennas, but we have in the past demonstrated that a 20 W coded continuous HF radar with transmitter and receiver separated by 500 m. This issue can potentially complicate the deployment of a meteor radar. It is also possible that a continuously operating transmission might saturate other sensitive radio receivers close by, even if they are not operating on the same frequency. However, with careful planning and surveying, these issues are not prohibitive.

6 Conclusions

We have described the concept of a coded CW specular meteor radar, which can be used to build a large scale multi-static network of meteor radars, in which each single frequency receiver can listen to all of the transmitters that are within vicinity. The only restriction is that the transmitter cannot be extremely close to the receiver.

Our measurement campaign results indicate that the 30 W coded CW meteor radar is nearly as sensitive as a standard pulsed meteor radar with 15 kW of peak power and

AMTD
8, 7879–7907, 2015

770 W of average power. The coded CW radar results pick up significantly less false detections due to RFI, which is apparent from Figs. 4, 5, and 6 that compare detections with the coded CW bi-static measurements and the pulsed bi-static measurements obtained using the same geometry and antennas.

The zonal and meridional winds derived with the coded bi-static CW meteor trail measurements agree well with the Collm mono-static pulsed meteor radar system, which indicates that the data quality is comparable, and could be used for MLT wind determination. Such coded CW systems would be a nice complement to the MMARIA concept presented by Stober and Chau (2015).

Even though we have focused on the use of the coded CW method for specular meteor radars in this study, we have already applied the same signal processing principles for vertical HF radar and ionosonde measurements. This type of a radar transmission principle would work well also with, e.g., the SuperDARN type of a HF over-the-horizon radar. Discussing these applications is a topic of future work. In these applications, the benefits of the method are similar: reduction of peak transmit power, removal of range-Doppler ambiguity, more tolerance to interference, more flexibility in spectral resolution, and the possibility to sound multiple channels with the same frequency simultaneously.

Acknowledgement. The authors would like to thank Dieter Keuer, Jens Mielich and Jörg Trautner for help with performing the measurements in Juliusruh and Kühlungsborn. We thank Christoph Jacobi for supporting the Collm Meteor Radar observations.

References

Chau, J., Strelnikova, I., Schult, C., Oppenheim, M., Kelley, M., Stober, G., and Singer, W.: Non-specular meteor trails from non-field-aligned irregularities: can they be explained by presence of charged meteor dust?, Geophys. Res. Lett., 41, 3336–3343, 2014. 7881, 7894

Dyrud, L. P., Oppenheim, M. M., Close, S., and Hunt, S.: Interpretation of non-specular radar meteor trails, Geophys. Res. Lett., 29, 8–1, 2002. 7881

Evans, J.: Radar observations of meteor deceleration, J. Geophys. Res., 71, 171–188, 1966. 7881

AMTD
8, 7879–7907, 2015

Evans, J. V. and Hagfors, T.: Radar Astronomy, edited by: Evans, J. V. and Hagfors, T., McGraw-Hill, New York, USA, 1, 1968. 7881

Frank, R.: Comments on "Polyphase codes with good periodic correlation properties" by Chu, D. C., Information Theory, IEEE T., 19, 244–244, 1973. 7886

Fritts, D., Janches, D., and Hocking, W.: Southern Argentina Agile Meteor Radar: initial assessment of gravity wave momentum fluxes, J. Geophys. Res.-Atmos., 115, D19123, doi:10.1029/2010JD013891, 2010. 7882

Hocking, W. K.: Temperatures Using radar-meteor decay times, Geophys. Res. Lett., 21, 3297–3300, doi:10.1029/1999GL003618, 1999. 7881

Hocking, W., Fuller, B., and Vandepeer, B.: Real-time determination of meteor-related parameters utilizing modern digital technology, J. Atmos. Sol.-Terr. Phy., 63, 155–169, 2001a. 7891, 7893

Hocking, W., Fuller, B., and Vandepeer, B.: Real-time determination of meteor-related parameters utilizing modern digital technology, J. Atmos. Sol.-Terr. Phy., 63, 155–169, 2001b. 7881

Hofmann-Wellenhof, B., Lichtenegger, H., and Collins, J.: Global Positioning System: Theory and Practice, Springer Science and Business Media, Vienna, Austria, 2013. 7882

Holdsworth, D. A., Reid, I. M., and Cervera, M. A.: Buckland Park all-sky interferometric meteor radar, Radio Sci., 39, RS5009, doi:10.1029/2003RS003014, 2004. 7881, 7891, 7892, 7893

Hysell, D. L. and Chau, J. L.: Inferring E region electron density profiles at Jicamarca from Faraday rotation of coherent scatter, J. Geophys. Res., 106, 30371, doi:10.1029/2000JA001101, 2001. 7894

Hysell, D. L., Larsen, M. F., and Zhou, Q. H.: Common volume coherent and incoherent scatter radar observations of mid-latitude sporadic E-layers and QP echoes, Ann. Geophys., 22, 3277–3290, doi:10.5194/angeo-22-3277-2004, 2004. 7894

Jacobi, C. A. D. K.: Long-period upper mesosphere temperature and plasma scale height variations derived from VHF meteor radar and LF absolute reflection height measurements, Adv. Radio Sci., 4, 351–355, 2006, http://www.adv-radio-sci.net/4/351/2006/. 7891

Janches, D., Hocking, W., Pifko, S., Hormaechea, J., Fritts, D., Brunini, C., Michell, R., and Samara, M.: Interferometric meteor head echo observations using the Southern Argentina Agile Meteor Radar, J. Geophys. Res.-Space, 119, 2269–2287, 2014. 7894

Jones, J., Webster, A., and Hocking, W.: An improved interferometer design for use with meteor radars, Radio Sci., 33, 55–65, 1998. 7890

AMTD
8, 7879–7907, 2015

Jones, J., Brown, P., Ellis, K., Webster, A., Campbell-Brown, M., Krzemenski, Z., and Weryk, R.: The Canadian Meteor Orbit Radar: system overview and preliminary results, Planet. Space Sci., 53, 413–421, doi:10.1016/j.pss.2004.11.002, 2005. 7881, 7882

Kozlovsky, A., Shalimov, S., Lukianova, R., and Lester, M.: Ionospheric effects of the missile destruction on 9 December 2009, J. Geophys. Res.-Space, 119, 3873–3882, 2014. 7894

Lehtinen, M. S. and Häggström, I.: A new modulation principle for incoherent scatter measurements, Radio Sci., 22, 625–634, 1987. 7882

Markkanen, J., Lehtinen, M., and Landgraf, M.: Real-time space debris monitoring with EISCAT, Adv. Space Res., 35, 1197–1209, 2005. 7881, 7889, 7894

McKinley, D. W. R.: Meteor Science and Engineering, McGraw-Hill, Toronto, Canada, 1961a. 7882

McKinley, D. W. R.: Meteor Science and Engineering, McGraw-Hill, New York, USA, 1, 1961b. 7880

Pellinen-Wannberg, A. and Wannberg, G.: Meteor observations with the European incoherent scatter UHF radar, J. Geophys. Res.-Space, 99, 11379–11390, 1994. 7881

Stober, G. and Chau, J. L.: A multistatic and multifrequency novel approach for specular meteor radars to improve wind measurements in the MLT region, Radio Sci., 50, 431–442, doi:10.1002/2014RS005591, 2015. 7882, 7883, 7890, 7896

Stober, G., Jacobi, C., Matthias, V., Hoffmann, P., and Gerding, M.: Neutral air density variations during strong planetary wave activity in the mesopause region derived from meteor radar observations, J. Atmos. Sol.-Terr. Phy., 74, 55–63, doi:10.1016/j.jastp.2011.10.007, 2012. 7893

Sugar, G. R.: Radio propagation by reflection from meteor trails, P. IEEE, 52, 116–136, 1964. 7880

Sulzer, M. P.: A radar technique for high range resolution incoherent scatter autocorrelation function measurements utilizing the full average power of klystron radars, Radio Sci., 21, 1033–1040, 1986. 7882, 7895

Vierinen, J., Lehtinen, M. S., Orispaa, M., and Virtanen, I. I.: Transmission code optimization method for incoherent scatter radar, Ann. Geophys., 26, 2923–2927, doi:10.5194/angeo-26-2923-2008, 2008. 7882, 7895

Virtanen, I. I., Lehtinen, M. S., Nygrén, T., Orispää, M., and Vierinen, J.: Lag profile inversion method for EISCAT data analysis, Ann. Geophys., 26, 571–581, doi:10.5194/angeo-26-571-2008, 2008. 7895

AMTD
8, 7879–7907, 2015

Volz, R. and Close, S.: Inverse filtering of radar signals using compressed sensing with application to meteors, Radio Sci., 47, RS0N05, doi:10.1029/2011RS004889, 2012. 7894
Woodman, R.: High-altitude-resolution stratospheric measurements with the Arecibo 2380-MHz radar, Radio Sci., 15, 423–430, 1980. 7882

AMTD
8, 7879–7907, 2015

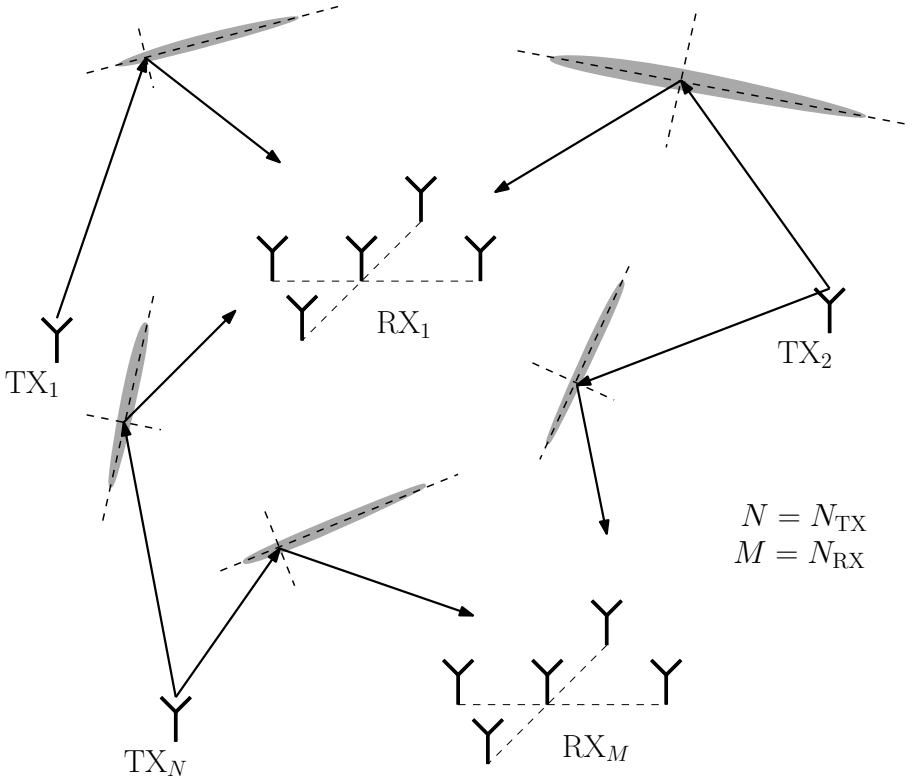

Figure 1. A depiction of a multi-static meteor radar network with multiple transmitters and multiple interferometric receivers. Each transmit-receiver pair observes meteors that match the specular condition, which is usually not met between two different transmit-receiver paths, and therefore to first order, each transmit-receiver path observes an independent set of meteor trails.

AMTD
8, 7879–7907, 2015

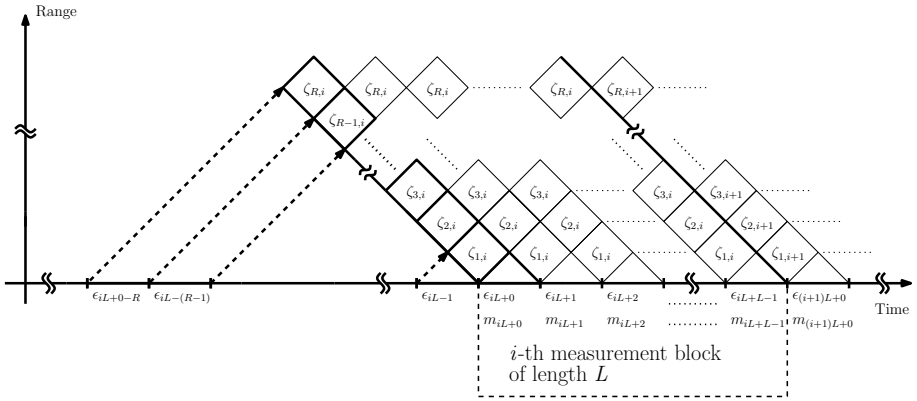

Figure 2. A range-time diagram describing the relation between coherence time, range gates, and the transmit envelope.

AMTD
8, 7879–7907, 2015

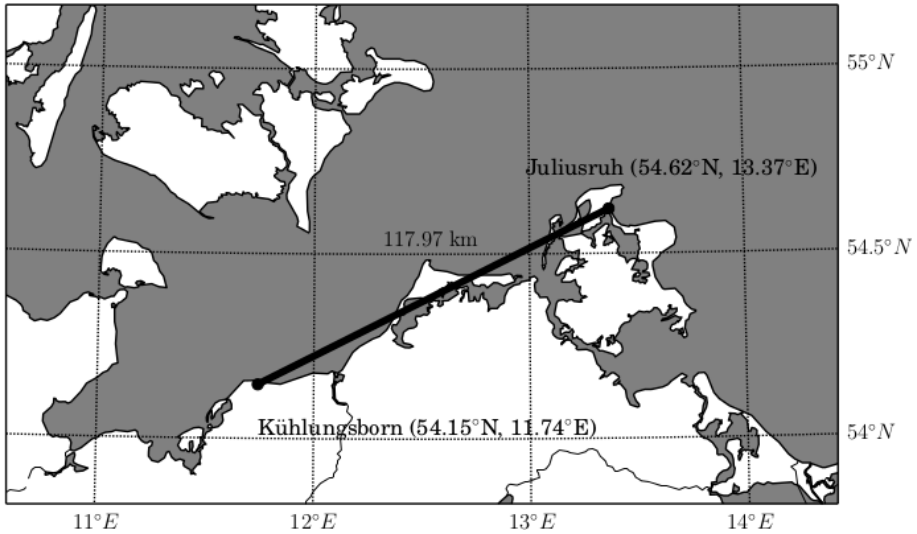

Figure 3. Geometry for the bi-static meteor radar experiment. The transmitter was located in Juliusruh, and the receiver was located at Kühlungsborn, a 118 km great circle distance from the transmitter.

AMTD
8, 7879–7907, 2015

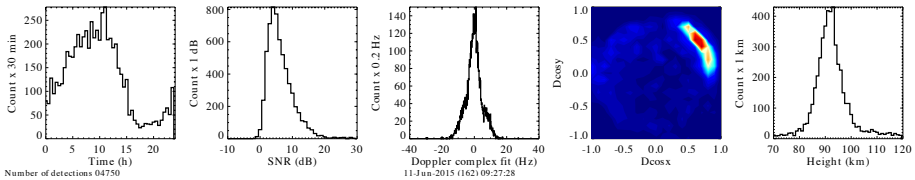

Figure 4. Summary results from coded CW specular meteor radar experiment for 24 h taken on 11 June 2015. **(a)** Count as function of day, **(b)** SNR histogram, **(c)** Doppler velocity histogram, **(d)** echo location bivariate histogram, and **(e)** altitude distribution.

AMTD
8, 7879–7907, 2015

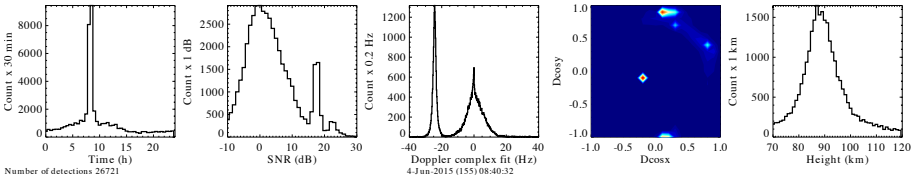

Figure 5. Same as Fig. 4, but for 24 h taken on 4 June 2015 with a standard pulsed system, on the same bistatic configuration. Note the presence of interference detected as possible meteors.

AMTD
8, 7879–7907, 2015

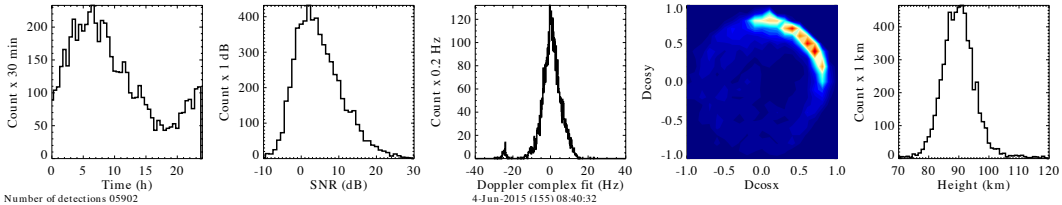

Figure 6. Same as Fig. 5, but with false detections that are considered to be caused by external inteference are removed, in addition to echoes that are considered to be from overdense meteor trails.

AMTD
8, 7879–7907, 2015

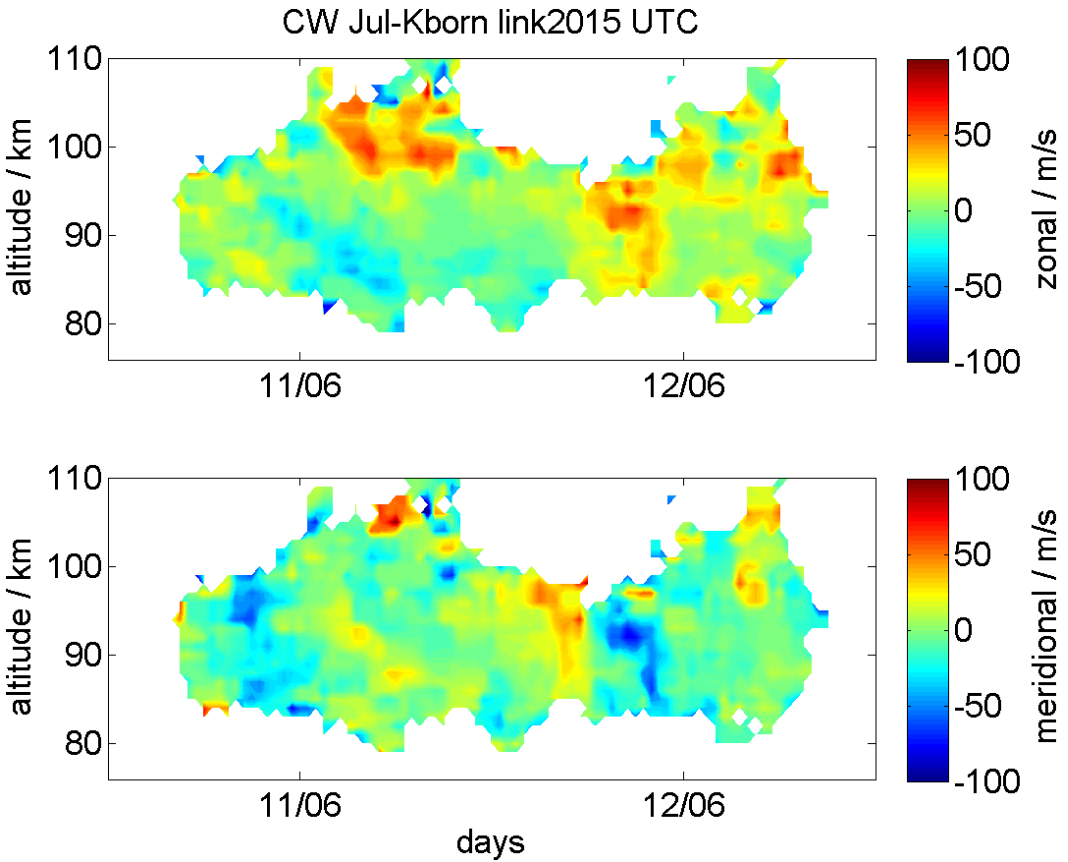

Figure 7. Zonal and meridional wind derived from the CW experiment using the forward scatter radio link between Juliusruh and Kühlungsborn.

AMTD
8, 7879–7907, 2015

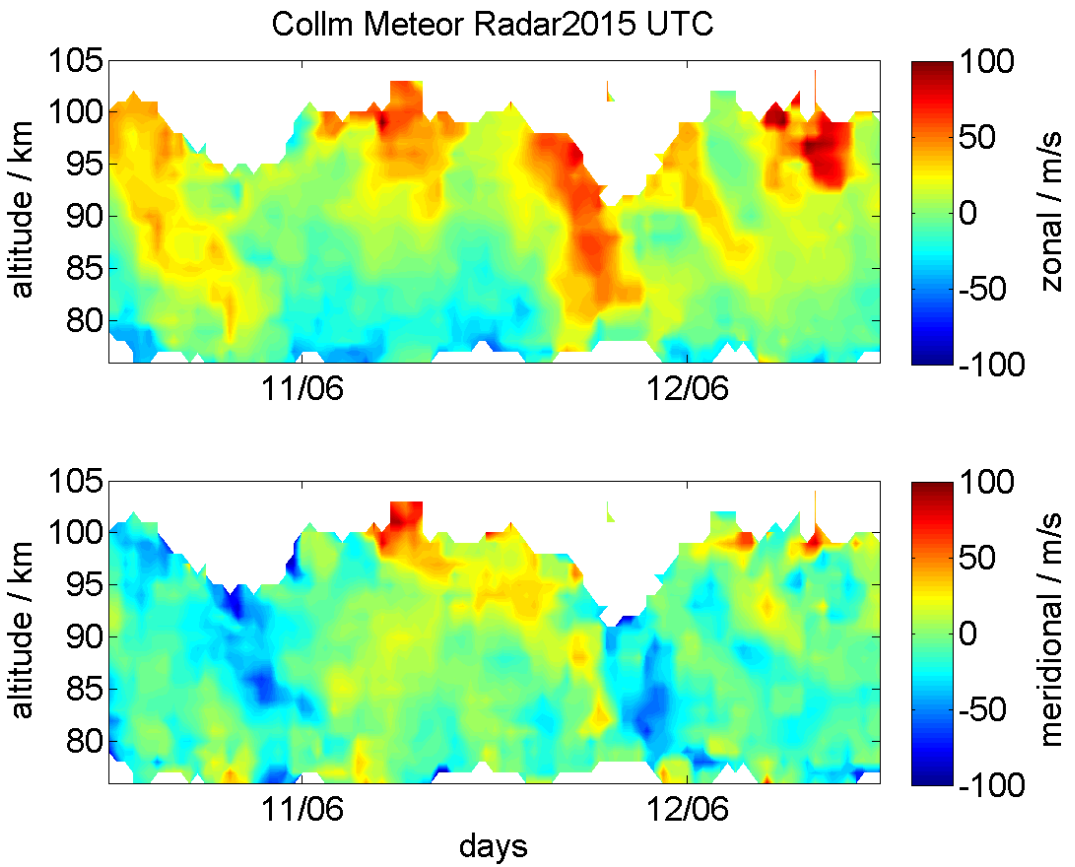

Figure 8. Zonal and meridional wind as observed by the Collm Meteor Radar approximately 350 km south of the CW radio link between Juliusruh and Kühlungsborn.

AMTD
8, 7879–7907, 2015